Bimetallic Nanocrystals

DOI: 10.1002/ange.201205279

Highly Branched Concave Au/Pd Bimetallic Nanocrystals with Superior Electrocatalytic Activity and Highly Efficient SERS Enhancement**

*Lin-Fei Zhang, Sheng-Liang Zhong, and An-Wu Xu**

With the development of research into nanomaterials, noble metal nanocrystals (NCs) have attracted wide interest because of their novel physical and chemical properties and promising applications in catalytic, plasmonics, electronics, surface-enhanced Raman scattering (SERS), and biomedicine.[1] The size- and shape-dependent properties of NCs have stimulated research into noble metal NCs of various shapes, such as wires, rods, prisms, plates, polyhedrons, and branched nanostructures.[1,2] Our interest is focused on branched NCs because their rough surfaces and possible high-index facets could be utilized for surface-sensitive applications, such as SERS and catalysis.[3] Their pronounced SERS efficiencies have been attributed to the presence of large numbers of tips and edges in highly branched metal NCs; these tips and edges can serve as hot spots for large electric-field enhancement, thus resulting in strong SERS signals. In fact, branched noble metallic NCs are also very efficient for electrocatalytic applications.[1–3] For instance, Au and Pd nanodendrites are excellent catalysts for the reduction of ferricyanide by thiosulfate,[4] ethanol electrooxidation,[5] etc. The superior catalytic activity of the branched NCs stems from the exposure of certain high-index facets that are intrinsically more-active towards specific reactions.

Synthetic approaches for preparing highly branched nanostructures of bimetallic NCs have not been explored as extensively as for monometallic NCs. Recently, limited success has been achieved in the preparation of bimetallic NCs with branched morphologies. Xia and co-workers prepared Pd–Pt bimetallic nanodendrites in the presence of uniform Pd nanocrystal seeds in an aqueous solution.[3a,b] The groups of Wang and Yamauchi developed a wet-chemical approach for the synthesis of high-quality three-dimensional Pt-on-Pd bimetallic nanodendrites at room temperature.[6] Although a number of noble metal branched NCs including Pt, Pd, Au, Ag, and some of their bimetallic combinations were prepared with concave surfaces,[7] to our knowledge, NCs with five-fold symmetric branches and concave surfaces have not been previously reported.

Herein, we describe the synthesis of highly branched concave Au/Pd bimetallic NCs with high-index facets by seed-mediated growth in aqueous solution at room temperature. We observe a large number of tips and edges in the highly branched concave structures and propose the growth mechanism for the evolution of this unique structure. The obtained branched Au/Pd bimetallic NCs exhibit much better catalytic activity than spherical Au/Pd catalysts. The plasmonic properties and SERS activities of the synthesized branched Au/Pd bimetallic NCs were also investigated, and these NCs showed high SERS enhancement.

For a typical synthesis of concave branched Au/Pd bimetallic nanostructures, the desired quantities of Na_2PdCl_4 and $HAuCl_4$ were introduced into a binary surfactant mixed solution, containing cetyltrimethylammonium chloride (CTAC) and didodecyldimethylammonium bromide (DDAB), in the presence of presynthesized rod-shaped Au/Pd nanoparticles with an aspect ratio of 2.0, as the seeds. The rod-shaped seed was composed of a Au core and Pd shell (see the Supporting Information, Figure S1). After $AgNO_3$, HCl, and ascorbic acid were added, the Au and Pd precursors were gradually co-reduced to Au and Pd atoms that were deposited on the Au/Pd seeds (see the Supporting Information for details). The UV/Vis extinction spectrum of the prepared Au/Pd seeds exhibits a single surface plasmon peak at 545 nm, which can be assigned to dipole plasmonic resonance (see the Supporting Information, Figure S1b). Figure 1a–c shows typical scanning electron microscopy (SEM) images of the as-prepared sample. It was found that over 90% of the synthesized Au/Pd NCs exhibited highly branched structures and displayed striking structures having concave branches of a uniform size. The morphology of the individual branched NCs is reminiscent of a starfish (inset in Figure 1c). The distance between each of the adjacent apices is approximately equal (300 nm), and the distance from the center to each apex is approximately 280 nm, as shown in Figure 1c, thus revealing its highly symmetric structure. The branches grow radially from a central core in five directions, thus suggesting that five-fold symmetric branches result from the five-fold symmetric growth. Figure 1d shows a low-magnification TEM image of the highly branched Au/Pd nanostructures, which are 550–700 nm in size; the particles display extensive branches.

[*] L. F. Zhang,[+] Prof. Dr. A. W. Xu
Division of Nanomaterials and Chemistry
Hefei National Laboratory for Physical Sciences at Microscale
University of Science and Technology of China
Hefei 230026 (China)
E-mail: anwuxu@ustc.edu.cn
L. F. Zhang,[+] Dr. S. L. Zhong[+]
College of Chemistry and Chemical Engineering
Jiangxi Normal University, Nanchang 330022 (China)
[+] These authors contributed equally to this work.

[**] We acknowledge support by the National Basic Research Program of China (2010CB934700, 2011CB933700) and the National Science Foundation of China (21271165).

Supporting information for this article is available on the WWW under http://dx.doi.org/10.1002/anie.201205279.

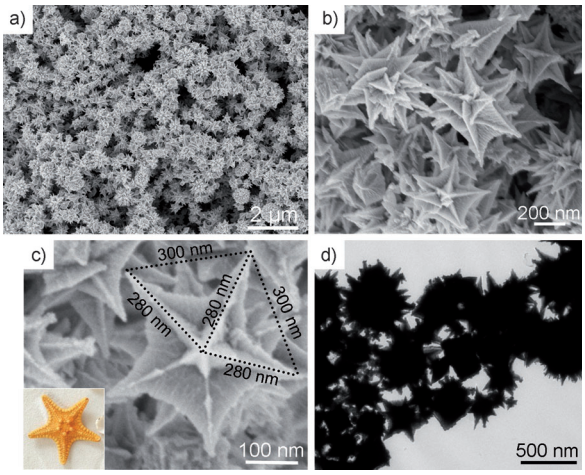

Figure 1. a,b) Low- and c) high-magnification SEM images of the concave branched Au/Pd bimetallic nanocrystals. d) Low-magnification TEM image of highly branched Au/Pd nanocrystals. The inset in (c) shows the photograph of a starfish.

Notably, this nanostar structure was not obtained in the absence of seeds (see the Supporting Information, Figure S2).

To better understand the crystalline characteristics of the branched Au/Pd nanostructure, high resolution TEM (HRTEM) measurements of a single nanostructure were performed. The sharp edges and corners of the branched structure can be easily identified (Figure 2a). A twinned {111} plane can be clearly observed in the HRTEM image (Figure 2b), thus indicating that the branched structures are twinned. As shown in the selected area of the electron diffraction pattern (SAED, inset in Figure 2b), the particles are single crystals, although some exhibit a high density of twin-like defects on {111} planes with a lattice spacing of 0.235 nm, as indicated in Figure 2b. Usually, the star-like five-fold twinned gold nanocrystals are notched at the {111} twin plane, which was reported to be the energetically favorable

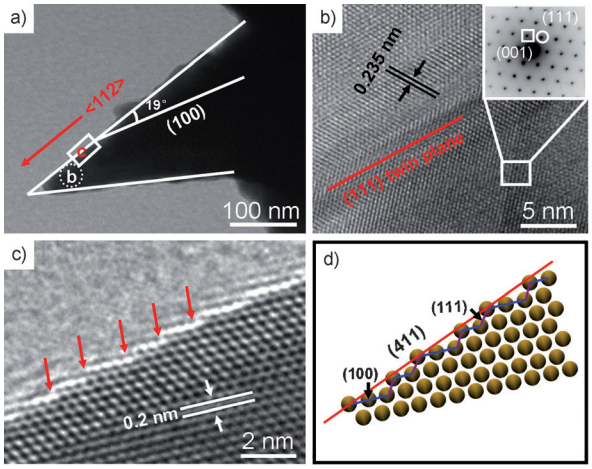

Figure 2. a) TEM image of one branch of an Au/Pd nanostar. b,c) HRTEM images taken from the region indicated within the boxes in (a). d) The atomic model of the {411} planes projected from the [110] zone axis and showing the (100) terraces and (111) steps. The inset of (b) shows the corresponding SAED pattern.

configuration,[8] thus driving the formation of the five-fold symmetric star structure. Notably, each branch of the stars observed in this study grows parallel to the {111} twin boundaries along the <112> direction. More-detailed HRTEM measurements (Figure 2c) confirm that the side face of a typical branch can be assigned to {411} facets according to the projection angle (19°) in the Figure 2a between the surface and the {100} facets (see the Supporting Information, Table S1 for more details). The arrows in Figure 2c point to atomic steps on the branch surface that create a series of alternating (100) and (111) sub-facets. These small facets are combined to form the high-index {411} facets. The atomic model of (411) planes with (100) terraces and (111) steps is shown in Figure 2d. The borders of each branch are not smooth, because small sub-facets are generated. More importantly, some branches possess a high density of low-coordinate atomic steps, such as {311}, {411}, {511}, and {611} steps, that can be identified on the borders (see the Supporting Information, Figures S3 and S4 for details). It is worth noting that these atomic steps are exposed on the branch surface, and can act as highly catalytic active sites.[6,9] Notably, the branches are spatially separated from each other, thus maximizing the surface area and preventing agglomeration.

Using our synthetic strategy, the size and morphology of the Au/Pd NCs can be readily tailored by controlling the amount of the reactants and the reaction time (see the Supporting Information, Figures S5–S9). Time-dependent experiments confirmed that the irregular nanostars of the Au/Pd NCs formed in only 30 min (Figure S5), and the particle size was about 60 nm. When the reaction time was prolonged to 3 h, nearly spherical and relatively rough Au/Pd NCs with a particle size of about 100 nm were obtained. By further increasing the reaction time, the branched shape of the Au/Pd NCs became more and more obvious and perfect, and the size of NCs gradually increased to reach 550–700 nm at 12 h (see the Supporting Information, Figure S5d–f). After 12 h, no significant change in the structure and morphology was observed. Energy dispersive spectra (EDS) analysis indicated that the Pd atomic content increased with increasing reaction time, from 16.3 (30 min) to 27.4 atomic% (12 h; see the Supporting Information, Figure S6). Such a change in the Pd atomic content could be due to the different reduction abilities of the Au and Pd precursors, thus resulting in different changes of precursor concentrations during the reaction. To monitor the growth of the concave branched Au/Pd NCs, in situ UV/Vis absorption spectra were recorded at different reaction times during the synthesis of the NCs (see the Supporting Information, Figure S7). A distinct absorption band at about 570 nm, which is ascribed to the surface plasmon resonance (SPR) of the irregular topography of the Au/Pd particles of about 60 nm in diameter, appeared and increased in intensity during the growth of the NCs. When the reaction time was increased to 12 h, the SPR peak of Au/Pd NPs gradually broadened and red-shifted from 570 nm to 740 nm owing to an increase in the particle size and aspect ratio of nanothorns.

Additional experiments showed that the Au/Pd molar ratios in the precursor solution play a key role in the formation of concave branched Au/Pd NCs. Using only

Na_2PdCl_4 or $HAuCl_4$ as the metal precursor resulted in microplates or nearly spherical shapes, respectively (see the Supporting Information, Figure S8a and S8f). When mixed metal precursors with Au/Pd molar ratios of 4:1, 3:2, and 1:1 were used, NCs with concave branched structures were generated (Figure 1 and the Supporting Information, Figure S8d–e), whereas the use of metal precursors with a Au/Pd molar ratio of 1:4 and 2:3 did not produce concave branched NCs (see the Supporting Information, Figure S8b–c). These results indicate that the co-reduction a suitable molar ratio of both metal precursors is necessary for the successful formation of concave Au/Pd branched NCs. This outcome can be attributed to the competitive reduction between the Au and Pd precursors that influences the kinetic growth of NCs.[10] To further investigate the importance of kinetic control of the reduction in the synthesis of concave branched Au/Pd NCs, the amount of reductant, ascorbic acid, was varied during the synthesis, while the other experimental conditions were kept constant. When 200 μL of either 1.0 M or 0.05 M aqueous solutions of ascorbic acid were used in the synthesis, concave branched Au/Pd NCs were not generated (see the Supporting Information, Figure S9a and S9c). Concave Au/Pd branched NCs were produced from solutions with an intermediate content of ascorbic acid (200 μL, 0.5 M; see the Supporting Information, Figure S9b). Our findings imply that use of the appropriate concentration of the reductant can facilitate the formation of highly branched concave Au/Pd NCs with high-index facets.

From the above experimental results, the structural evolution of the branched Au/Pd nanostructures with a concave surface in an aqueous solution suggests that the five-fold symmetric particle growth occurs in the presence of multiple twinning. For instance, it has been reported that the stress/strain release effects during the growth of Au NCs can give rise to branched nanostructures.[11] Factors such as forced reduction of Au ions have also been proposed to play a key role in the growth of branched metal NCs.[12] Multiple twinning, which often occurs in noble metal NCs owing to their low twinning energies,[13] has previously been observed in Au nanorods, bipyramids, and polyhedra.[14]

In the present case, TEM and HRTEM measurements of the particles obtained after the first 30 min of the reaction indeed show five-fold twinned boundaries (marked by arrows, Figure 3a and b), which are also confirmed by the SAED pattern (inset in Figure 3b). The branches of the Au/Pd NCs observed in our study grow parallel to the {111} twin boundaries along the ⟨112⟩ direction. In general, there are two different types of corners for five-fold twinned NCs, for example A and B, as labeled in Figure 3c. Assuming that perfect twinned planes are formed, the growth along corners A and B is in the ⟨112⟩ and ⟨110⟩ direction, respectively. The emergence of star-like Au/Pd NCs with five branches implies that growth along the ⟨112⟩ direction is more rapid than that in the ⟨110⟩ direction.[15] In this study, it is assumed that the cooperative interactions of $AgNO_3$, CTAC, and DDAB determine the growth rate of the different planes and thereby can promote the excessive growth along ⟨112⟩. The presence of Ag ions has been used in other seed-mediated syntheses to stabilize high-index facets through a so-called underpotential

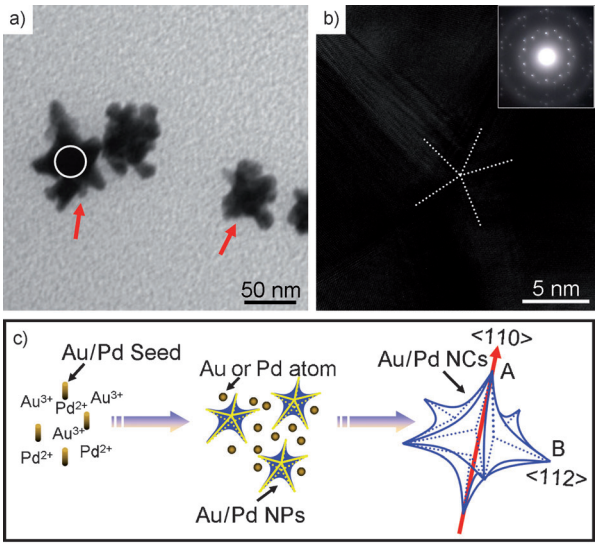

Figure 3. a) TEM image of the product obtained after reaction for 30 min. b) HRTEM image taken from the white circle of the nanoparticle shown in (a). Inset shows the corresponding SAED pattern. c) Schematic view of the development of branched Au/Pd fivefold symmetric NCs from multiply twinned units (a penta-twinned unit is formed from five tetrahedral units). A and B represent the growth direction along ⟨110⟩ and ⟨112⟩, respectively.

deposition (UPD) mechanism. The presence of Cl^- significantly influences the UPD behavior of Ag onto Au, with Ag being deposited specifically onto atomic steps below a Cl or Br adlayer, thus making the removal of Ag more difficult.[16] Although both CTAB or DDAB, and mixtures of these with CTAC have been used in the synthesis of nanostructures with high-index facets, the presence of CTAC has been attributed to the generation of metal NCs with a star-like shape.[17] Efforts aimed at understanding the role of the halide in the particle growth pathway are underway. Nevertheless, a saturation of the halide might lead to crystal growth along the plane of the defects, that is, the twin boundaries. The weak bonding in twin boundary regions provides sites for Au and Pd atom diffusion to these sites.[18] In fact, branched concave NCs were not produced in the absence of any of the reagents ($AgNO_3$, CTAC and DDAB; Figure S10). Based on the above facts, we propose the following growth mechanism to explain the evolution of twinned surface branches in our case (Figure 3c). Initially, Au and Pd atoms are deposited onto the defect regions of the Au/Pd NPs to form small twinned protrusions, which grow into distinct branches on the surface and further transform into well-defined branched Au/Pd nanostars, having concave surfaces as well as high-index facets, owing to the synergistic effects of $AgNO_3$, CTAC, and DDAB, and stabilization by binary surfactants.

As mentioned above, the highly branched Au/Pd NCs are expected to exhibit efficient surface-enhanced Raman spectra (SERS) and superior electrocatalytic activity owing to the presence of a large number of hot spots, sharp multitips, edges, and nanoparticle interfaces as well as high-energy step atoms on their concave surfaces. The SERS response was examined by using crystal violet (CV) dye as the probe molecule. CV was selected because of its distinct Raman

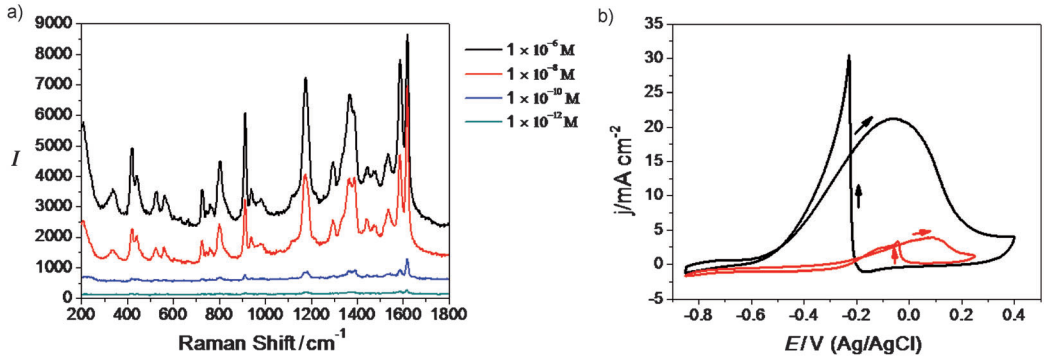

Figure 4. a) SERS spectra of crystal violet adsorbed on the concave branched Au/Pd bimetallic nanocrystals. The SERS spectra were obtained with $\lambda_{ex} = 514$ nm excitation, $P_{laser} = 1$ mW, and $t = 20$ s. b) Cyclic voltammetry curves measured for the branched Au/Pd bimetallic NCs and spherical Au/Pd bimetallic NCs in an N_2-purged 0.1 M KOH + 0.5 M ethanol solution at a scan rate of 50 mV s^{-1}.

features and its ability to form a self-assembled monolayer or sub-monolayer on Au/Pd particles without any further chemical modification.[3,19] A series of solutions with dye concentrations ranging from 10^{-6} to 10^{-12} M were prepared in deionized water. The samples used for SERS measurement were prepared by placing a 10 μL droplet onto the Teflon film and allowing evaporation in air. Typical SERS spectra from the different concentrations of dye on the Teflon films are shown in Figure 4a. Well-resolved peaks were obtained at concentrations as low as 10^{-12} M (see the Supporting Information, Figure S11). The SERS capability of the branched Au/Pd NCs was evaluated by estimating the enhancement factor (EF) by the approach developed by Le Ru et al.[20] The SERS EFs were estimated to be 1.12×10^7 (details given in Supporting Information) based on the intensity ratio of the typical scattering band at approximately 1617 cm^{-1} from SERS and normal Raman spectra of CV. The branched Au/Pd NCs contain many intra- and interparticle gaps, tips, and edges, which are supposed to be rich in hot spots, thus giving the strong SERS signals at extremely low concentrations.

Au/Pd bimetallic alloy and core-shell NCs have been widely studied because of their excellent catalytic efficiencies for a variety of chemical reactions.[7,10,21] In particular, Pd-based catalysts provide a higher electrocatalytic activity toward ethanol oxidation than Pt in alkaline solutions.[22] As there are high-density atomic steps on {h11} high-index surfaces, our concave branched Au/Pd bimetallic NCs are expected to exhibit high electrocatalytic activity. For comparison, the electrocatalytic properties of the spherical Au/Pd bimetallic NCs obtained when the concentration of ascorbic acid was 1.0 M (see the Supporting Information, Figure S9a) were also measured under the same conditions. Figure 4b shows cyclic voltammogram (CV) curves of the ethanol oxidation activities of the two different NCs in a 0.1 M KOH with 0.5 M ethanol solution. The catalytic activity of the branched Au/Pd NC is superior to that of the spherical Au/Pd NC catalyst. The peak current densities of ethanol oxidation on the branched Au/Pd NCs for the potential scans in the positive and negative direactions are 21.30 and 31.25 mA cm^{-2}, respectively. Corresponding current densities obtained for the spherical Au/Pd NCs catalyst are 3.71 and 3.53 mA cm^{-2}. The concave Au/Pd branched NCs with {h11} high-index facets exhibit 7–8 times higher catalytic activity per unit surface area towards the electrooxidation of ethanol in an alkaline solution than the spherical Au/Pd NCs catalyst. The mass normalized current density of our branched Au/Pd nanostars in the positive direction sweep (1.065 A (mg of AuPd)$^{-1}$) was about 9 times higher than that of commericially available Pt black (0.11 A (mg of Pt)$^{-1}$), when measured under the same conditions.[6] The higher electrocatalytic ability of the branched Au/Pd bimetallic NCs primarily originates from the synergistic effects of the high-index {h11} facets, a lot of active sites (edges, corners). Moreover, the open structure of the Au/Pd nanostars is highly beneficial for the use as an electrocatalyst mainly because of their superior tolerance to undesirable agglomeration of the active sites.

In summary, highly branched concave Au/Pd bimetallic NCs have been prepared in high yield by facile seed-mediated growth. The reaction parameters are critical for the formation of these striking branched Au/Pd NCs. The importance of controlling the NCs five-fold symmetric growth to achieve the final products with the interesting nanostructures is shown. The concave branched Au/Pd NCs exhibit a high enhancement of SERS and also show much better electrocatalytic activity toward ethanol oxidation than spherical Au/Pd NCs and commercially available Pt black. Owing to the unique structure and properties, the synthesized NCs could find promising applications in the fabrication of novel highly active electrocatalysts for applications in fuel cell.

Received: July 5, 2012
Published online: November 28, 2012

Keywords: Au/Pd nanocrystals · concave surfaces · electrocatalysts · high-index facets · SERS

[1] a) Y. Xia, Y. Xiong, B. Lim, S. E. Skrabalak, *Angew. Chem.* **2009**, *121*, 62; *Angew. Chem. Int. Ed.* **2009**, *48*, 60; b) C. Burda, X. Chen, R. Narayanan, M. A. El-Sayed, *Chem. Rev.* **2005**, *105*, 1025; c) J. E. Millstone, W. Wei, M. R. Jones, H. Yoo, C. A. Mirkin, *Nano Lett.* **2008**, *8*, 2526; d) W. G. Qu, B. Deng, S. L. Zhong, H. Y. Shi, S. S. Wang, A. W. Xu, *Chem. Commun.* **2011**,

47, 1237; e) Y. W. Jun, J. S. Choi, J. Cheon, *Angew. Chem.* **2006**, *118*, 3492; *Angew. Chem. Int. Ed.* **2006**, *45*, 3414.

[2] a) J. Chen, B. Wiley, Z. Li, D. Campbell, F. Saeki, H. Cang, L. Au, J. Lee, X. Li, Y. N. Xia, *Adv. Mater.* **2005**, *17*, 2255; b) H. Lee, S. E. Habas, S. Kweskin, D. Butcher, G. A. Somorjai, P. D. Yang, *Angew. Chem.* **2006**, *118*, 7988; *Angew. Chem. Int. Ed.* **2006**, *45*, 7824; c) J. Chen, B. Lim, E. P. Lee, Y. N. Xia, *Nano Today* **2009**, *4*, 81; d) C. Salzemann, W. Zhai, N. Goubet, M. P. Pileni, *J. Phys. Chem. Lett.* **2010**, *1*, 149.

[3] a) B. Lim, M. Jiang, P. H. C. Camargo, E. C. Cho, J. Tao, X. Lu, Y. Zhu, Y. Xia, *Science* **2009**, *324*, 1302; b) J. Chen, T. Herricks, Y. Xia, *Angew. Chem.* **2005**, *117*, 2645; *Angew. Chem. Int. Ed.* **2005**, *44*, 2589; c) J. Watt, S. Cheong, M. F. Toney, B. Ingham, J. Cookson, P. T. Bishop, R. D. Tilley, *ACS Nano* **2010**, *4*, 396; d) J. X. Fang, S. Y. Du, S. Lebedkin, Z. Y. Li, R. Kruk, M. Kappes, H. Hahn, *Nano Lett.* **2010**, *10*, 5006; e) M. J. Mulvihill, X. Y. Ling, J. Henzie, P. D. Yang, *J. Am. Chem. Soc.* **2010**, *132*, 268.

[4] M. A. Mahmoud, C. E. Tabor, M. A. El-Sayed, Y. Ding, Z. L. Wang, *J. Am. Chem. Soc.* **2008**, *130*, 4590.

[5] a) Z. Yin, H. Zheng, D. Ma, X. Bao, *J. Phys. Chem. C* **2009**, *113*, 1001; b) F. Wang, C. H. Li, L. D. Sun, H. S. Wu, T. A. Ming, J. F. Wang, J. C. Yu, C. H. Yan, *J. Am. Chem. Soc.* **2011**, *133*, 1106; c) Y. Yu, Q. B. Zhang, B. Liu, J. Y. Lee, *J. Am. Chem. Soc.* **2010**, *132*, 18258.

[6] a) S. J. Guo, S. J. Dong, E. Wang, *ACS Nano* **2010**, *4*, 547; b) L. Wang, Y. Nemoto, Y. Yamauchi, *J. Am. Chem. Soc.* **2011**, *133*, 9674.

[7] a) X. Q. Huang, Z. P. Zhao, J. M. Fan, Y. M. Tan, N. F. Zheng, *J. Am. Chem. Soc.* **2011**, *133*, 4718; b) J. Zhang, M. R. Langille, M. L. Personick, K. Zhang, S. Li, C. A. Mirkin, *J. Am. Chem. Soc.* **2010**, *132*, 14012; c) X. H. Xia, J. Zeng, B. McDearmon, Y. Q. Zheng, Q. G. Li, Y. N. Xia, *Angew. Chem.* **2011**, *123*, 12750; *Angew. Chem. Int. Ed.* **2011**, *50*, 12542; d) C. L. Lu, K. S. Prasad, H. L. Wu, J. A. Ho, M. H. Huang, *J. Am. Chem. Soc.* **2010**, *132*, 14546; e) C. J. DeSantis, A. A. Peverly, D. G. Peters, S. E. Skrabalak, *Nano Lett.* **2011**, *11*, 2164; f) H. Zhang, M. S. Jin, Y. N. Xia, *Angew. Chem.* **2012**, *124*, 7774; *Angew. Chem. Int. Ed.* **2012**, *51*, 7656.

[8] a) X. Huang, X. Y. Qi, Y. Z. Huang, S. Z. Li, C. Xue, C. L. Gan, F. Boey, H. Zhang, *ACS Nano* **2010**, *4*, 6196; b) T. K. Sau, A. L. Rogach, M. Döblinger, J. Feldmann, *Small* **2011**, *7*, 2188.

[9] a) Z. Y. Zhou, Z. Z. Huang, D. J. Chen, Q. Wang, N. Tian, S. G. Sun, *Angew. Chem.* **2010**, *122*, 421; *Angew. Chem. Int. Ed.* **2010**, *49*, 411; b) S. W. Lee, S. Chen, W. C. Sheng, N. Yabuuchi, Y. Kim, T. Mitani, E. Vescovo, Y. Shao-Horn, *J. Am. Chem. Soc.* **2009**, *131*, 15669.

[10] a) Y. W. Lee, M. Kim, S. W. Kang, S. W. Han, *Angew. Chem.* **2011**, *123*, 3528; *Angew. Chem. Int. Ed.* **2011**, *50*, 3466; b) Y. A. Liu, R. H. Walker, *Angew. Chem.* **2010**, *122*, 6933; *Angew. Chem. Int. Ed.* **2010**, *49*, 6781; c) L. Zhang, D. Q. Chen, Z. Y. Jiang, J. W. Zhang, S. F. Xie, Q. Kuang, Z. X. Xie, L. S. Zheng, *Nano Res.* **2012**, *5*, 181.

[11] a) S. Chen, Z. L. Wang, J. Ballato, S. H. Foulger, D. L. Carroll, *J. Am. Chem. Soc.* **2003**, *125*, 16186; b) E. Ye, K. Y. Win, H. R. Tan, M. Lin, C. P. Teng, A. Mlayah, M. Y. Han, *J. Am. Chem. Soc.* **2011**, *133*, 8506; c) Z. Q. Li, W. Y. Li, P. H. C. Camargo, Y. N. Xia, *Angew. Chem.* **2008**, *120*, 9799; *Angew. Chem. Int. Ed.* **2008**, *47*, 9653.

[12] a) O. Krichevski, G. Markovich, *Langmuir* **2007**, *23*, 1496; b) M. Yamamoto, Y. Kashiwagi, T. Sakata, H. Mori, M. Nakamoto, *Chem. Mater.* **2005**, *17*, 5391; c) C. J. Johnson, E. Dujardin, S. A. Davis, C. J. Murphy, S. Mann, *J. Mater. Chem.* **2002**, *12*, 1765.

[13] T. K. Sau, A. L. Rogach, *Adv. Mater.* **2010**, *22*, 1781.

[14] a) M. Liu, P. Guyot-Sionnest, *J. Phys. Chem. B* **2005**, *109*, 22192; b) P. Jiang, J. J. Zhou, R. Li, Z. L. Wang, S. S. Xie, *Nanotechnology* **2006**, *17*, 3533; c) D. Seo, C. I. Yoo, I. S Chung, S. M. Park, S. Ryu, H. Song, *J. Phys. Chem. C* **2008**, *112*, 2469; d) L. F. Zhang, L. Wang, S. L. Zhong, Y. X. Huanga, A. W. Xu, *Dalton Trans.* **2012**, *41*, 4948.

[15] M. Tsuji, P. Jiang, S. Hikino, S. Lim, R. Yano, S. M. Jang, S. H. Yoon, N. Ishigami, X. Tang, K. Sozana, K. S. N. Kamarudin, *Colloids Surf. A* **2008**, *317*, 23.

[16] a) J. H. Lee, I. W. Oh, S. P. Hwang, J. Y. Kwak, *Langmuir* **2002**, *18*, 8025; b) R. Michalitsch, B. J. Palmer, P. E. Laibinis, *Langmuir* **2000**, *16*, 6533.

[17] a) Y. Y. Ma, Q. Kuang, Z. Y. Jiang, Z. X. Xie, R. B. Huang, L. S. Zheng, *Angew. Chem.* **2008**, *120*, 9033; *Angew. Chem. Int. Ed.* **2008**, *47*, 8901; b) T. Ming, W. Feng, Q. Tang, F. Wang, L. D. Sun, J. F. Wang, C. H. Yan, *J. Am. Chem. Soc.* **2009**, *131*, 16350; c) H. L. Wu, C. H. Chen, M. H. Huang, *Chem. Mater.* **2009**, *21*, 110.

[18] P. L. Gai, M. A. Harmer, *Nano Lett.* **2002**, *2*, 771.

[19] a) C. Chenal, R. L. Birke, J. R. Lombardi, *ChemPhysChem* **2008**, *9*, 1617; b) K. J. Khajehpour, T. Williams, L. Bourgeois, S. Adelojua, *Chem. Commun.* **2012**, *48*, 5349.

[20] E. C. LeRu, E. Blackie, M. Meyer, P. G. Etchegoin, *J. Phys. Chem. C* **2007**, *111*, 13794.

[21] a) L. Zhang, J. W. Zhang, Q. Kuang, S. F. Xie, Z. Y. Jiang, Z. X. Xie, L. S. Zheng, *J. Am. Chem. Soc.* **2011**, *133*, 17114; b) J. W. Hong, D. H. Kim, Y. W. Lee, M. J. Kim, S. W. Kang, S. W. Han, *Angew. Chem.* **2011**, *123*, 9038; *Angew. Chem. Int. Ed.* **2011**, *50*, 8876; c) G. J. Hutchings, *Chem. Commun.* **2008**, 1148.

[22] C. Bianchini, P. K. Shen, *Chem. Rev.* **2009**, *109*, 4183.

